Solution Structure and Functional Ligand Screening of HI0719, a Highly Conserved Protein from Bacteria to Humans in the YjgF/YER057c/UK114 Family[†,‡]

Lisa Parsons, Nicklas Bonander, Edward Eisenstein, Michael Gilson, Visvaldas Kairys, and John Orban*

Center for Advanced Research in Biotechnology, University of Maryland Biotechnology Institute, 9600 Gudelsky Drive, Rockville, Maryland 20850

Received August 19, 2002; Revised Manuscript Received October 28, 2002

ABSTRACT: HI0719 belongs to a large family of highly conserved proteins with no definitive molecular function and is found in organisms ranging from bacteria to humans. We describe the NMR structure of HI0719, the first solution structure for a member of this family. The overall fold is similar to the crystal structures of two homologues, YabJ from *Bacillus subtilis* and YjgF from *Escherichia coli,* and all three structures are similar to that of chorismate mutase, although there is little sequence homology and no apparent functional connection. HI0719 is a homotrimer with a distinct cavity located at the subunit interface. Six of the seven invariant residues in the high identity group of proteins are located in this cavity, suggesting that this may be a binding site for small molecules. Using previously published observations about the biological role of HI0719 family members as a guide, over 100 naturally occurring small molecules or structural analogues were screened for ligand binding using NMR spectroscopy. The targeted screening approach identified six compounds that bind to HI0719 at the putative active site. Five of these compounds are either α-keto acids or α,*β*-unsaturated acids, while the sixth compound is structurally similar. Previous studies have proposed that some HI0719 homologues may act on small molecules in the isoleucine biosynthetic path and, if this is correct, the ligand screening results presented here suggest that the interaction most likely occurs with 2-ketobutyrate and/or its unstable enamine precursor.

HI0719 belongs to a family of proteins for which there have been over 200 sequence relatives found to date, and these are widely distributed in bacteria, archaea, plants, and eukaryotes (see http://s2f.umbi.umd.edu/). A simple analysis of the level of sequence homology within this family reveals that these proteins can be divided into low identity and high identity groups in which the high identity group consists of proteins with approximately 38% sequence identity or better (Figure 1). Currently, this high identity group contains about 80 proteins and is known generally as the YjgF/YER057c/UK114 family. A sequence alignment for representative members of the high identity group is shown in Figure 2.

A wide variety of biological roles have been ascribed to members of the high identity group depending on the organism. Many of the proteins in this group have been annotated as putative translation inhibitors based on experiments with the human and rat homologues, hp14.5 and rp14.5 (also known as PSP1 or L-PSP), respectively, which both inhibited cell-free protein synthesis in the rabbit reticulocyte lysate system (*1*). Further studies with the rat homologue suggested that this inhibition was due to an endoribonuclease activity where rp14.5 cleaved single-stranded mRNA templates and led to disaggregation of the reticulocyte polysomes into 80S ribosomes (*2*). These effects were reported for both isolated and recombinant protein, although other studies have shown that the isolated versions are more active by 10−1000-fold (*1*, *3*). The yeast homologues, YIL051c and Yeo7, appear to play dual roles in mitochondrial maintenance and in the regulation of isoleucine biosynthesis (*4*, *5*). The bacterial homologue from *Lactococcus lactis*, aldR, is also implicated in isoleucine biosynthesis (*6*), and the gene for an *Escherichia coli* K-12 strain homologue, tdcF, resides on an operon responsible for the anaerobic degradation of threonine to propanoate (*7*). Other biological roles, such as calpain activation in the bovine homologue (*8*), tumor antigen activity in the goat homologue (*9*), and a role in purine

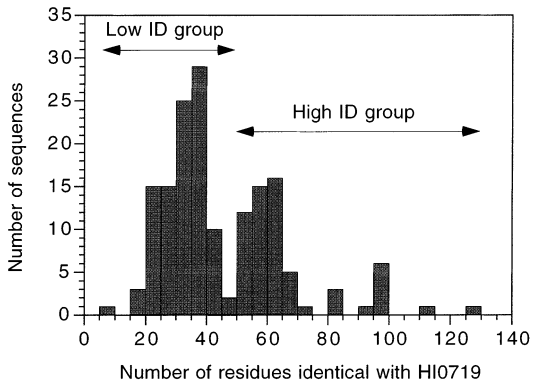

FIGURE 1: Plot showing the distribution of sequence identities (*x*-axis) versus the number of sequences with that level of sequence identity (*y*-axis) in the HI0719 family. Data were obtained from PSI−BLAST (*61*) output summarized at http://s2f.umbi.umd.edu/.

[†] Supported by NIH Grant GM57890. L.P. is a member of the Molecular and Cell Biology Graduate Program at University of Maryland College Park and is the recipient of a Life Technologies Fellowship.

[‡] The coordinates have been deposited in the Protein Data Bank (accession code 1J7H).

* To whom correspondence should be addressed. Ph: 301-738-6221; FAX: 301-738-6255; e-mail: orban@umbi.umd.edu.

10.1021/bi020541w CCC: $25.00
Published on Web 12/10/2002

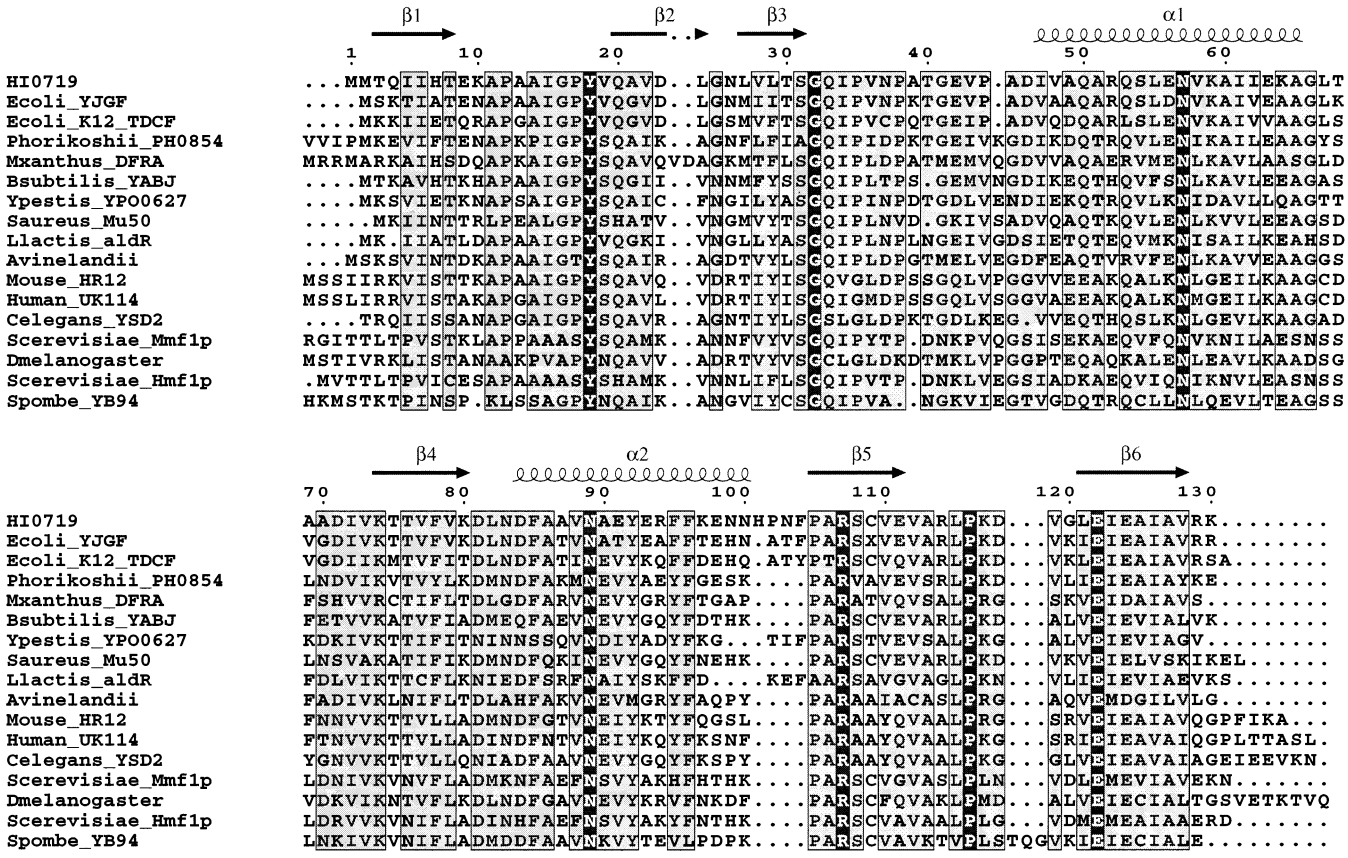

FIGURE 2: Alignment of representative sequences in the high identity group. Invariant residues are shown in dark columns and conserved residues are shown in gray columns. Sequence alignment was carried out with CLUSTALW (*62*) and displayed using ESPript (http://prodes.toulouse.inra.fr/).

regulation in *Bacillus subtilis* (*10*) have been reported or proposed. Further studies on yjgF null mutants in *Salmonella typhimurium* suggest phenotypic effects related to both the isoleucine biosynthetic path and the pentose phosphate path (*11*).

The structures of three high identity homologues, YjgF (76% identity on 129 residues) from *E. coli* (*12*), YabJ (48% identity on 128 residues) from *B. subtilis* (*13*), and Yeo7 (41% identity on 122 residues) from yeast (*14*) have been determined by X-ray crystallography. The crystal structures of YjgF and YabJ are homotrimers, while that of Yeo7 is a dimer of trimers and the trimeric arrangements in these structures are similar. In contrast, earlier reports claimed that the rat homologue, rp14.5 (PSP), was a dimer from size exclusion chromatography (*15*). Comparison of the YjgF and YabJ structures with those in the Protein Data Bank reveals that they are most similar to chorismate mutase (*16*) which is also a homotrimer. However, there is very little sequence homology (<10%) and no structural basis for chorismate mutase activity (*13*).

Despite the biological and structural observations reported and the widespread occurrence of this protein family, no definitive molecular function has yet been determined for proteins in the high identity group. The only unambiguous biochemical function to be found in this protein family is for three related low identity group members from *Pseudomonas putida*, *P. pseudoalcaligenes*, and *Pseudomonas* sp. AP-3. These proteins have an approximately 30% level of sequence identity with HI0719 and are 2-aminomuconate deaminases which occur in the nitrobenzene degradative pathway of these organisms (*17*−*20*). The overall fold of these proteins is likely to be similar to those in the high identity group, and the oligomeric state has been determined to be hexameric by size exclusion chromatography (*18*).

Here, we describe the first three-dimensional structure in solution for a member of the high identity group, HI0719 from *Haemophilus influenzae*, and evaluate potential biochemical functions for this protein. This is done using previously published observations as a guide for screening candidate ligands using NMR[1] spectroscopy (*21*).

MATERIALS AND METHODS

Sample Preparation. The gene for HI0719 was obtained from *Haemophilus influenzae* genomic DNA and inserted into the pET-15b and pET-17b vectors (Novagen) using *Nde*I and *Bam*HI restriction sites. The sequence was verified by DNA sequencing. Unlabeled, ^{15}N-labeled, and ^{15}N/^{13}C-labeled $(His)_6$ tagged protein (HI0719-his) from the pET-15b vector was purified as described previously (*22*). A typical yield of ^{15}N-labeled protein was 30 mg/L of fermentation culture.

Unless otherwise stated, all protein samples used for NMR were prepared from the pET-15b plasmid and concentrated to 1.5 mM. The final buffer conditions were 50 mM sodium phosphate, 100 mM NaCl, and 3 mM DTT, pH 6.7, in 10%

[1] Abbreviations: BLAST, basic local alignment search tool; CNS, crystallography and NMR system; HSQC, heteronuclear single quantum coherence; NMR, nuclear magnetic resonance; NOESY, nuclear Overhauser effect spectroscopy; TOCSY, total correlation spectroscopy.

D_2O and 90% H_2O. Hydrogen−deuterium (H−D) exchange experiments were carried out on a ^{15}N-labeled sample that was lyophilized and then dissolved in 99.9% D_2O. To identify intersubunit NOEs, a sample consisting of a 1:1 mixture of ^{15}N-labeled protein and $^{15}N/^{13}C$-labeled protein was equilibrated for 2 weeks at 4 °C. The sample was lyophilized and then dissolved in 99.9% D_2O to a final protein concentration of 3 mM.

Determination of Oligomeric State. (a) Native Gel Analysis. A solution containing 0.2 mM HI0719-his was mixed with 4 ng/mL of thrombin in 50 mM sodium phosphate, 100 mM NaCl, and 1 mM DTT at pH 6.7 (buffer A) and incubated at room temperature. Aliquots were taken at 0, 5, 10, 15, 20, and 30 min and put on ice. Samples were mixed 1:1 with 0.1% bromophenol blue in 50 mM Tris and 10% glycerol at pH 6.8 and loaded onto a 20% polyacrylamide native phastgel (Amersham Biosciences). Controls for the experiment were a 0.2 mM solution of HI0719-his in buffer A and a 0.2 mM solution of HI0719 cloned without the $(His)_6$ tag in buffer A.

(b) Light Scattering. Twenty-microliter samples were injected onto a Superose 6 gel filtration column attached to an Agilent 1100 series HPLC, and light scattering and concentration measurements were made using a DAWN EOS 18-angle light scattering detector (Wyatt Technology) and an OPTILAB DSP interferometric refractometer (Wyatt Technology). The column was equilibrated in 10 mM HEPES, 100 mM KCl, 0.2 mM EDTA, and 0.02% sodium azide at pH 7.50. A refractive index increment of 0.185 mL/g was used to estimate concentrations for molecular weight estimates, and bovine serum albumin was used as an isotropic scatterer for detector normalization to compensate for slight differences in the electronic gain of the 18 detectors. Molecular mass calculations were performed using ASTRA software (Wyatt Technology).

NMR Spectroscopy. NMR spectra were recorded at 308 K on Bruker DRX-500 and DRX-600 spectrometers equipped with 3-axis gradient probes. Spectra were recorded in States-TPPI mode with the use of pulsed-field gradients for coherence selection and solvent suppression (*23*). Sequence-specific main chain assignments were completed using ^{15}N HSQC (*24*), HNCO (*25*), HNCACB (*26*), and CBCA(CO)-NH (*27*) experiments. Side-chain assignments were obtained from ^{13}C CT-HSQC (*28*), HBHA(CO)NH (*27*), HCCH-COSY (*29*), HCCH-TOCSY (*30*) (DIPSI-3, τ_m 21 ms), and ^{15}N-edited TOCSY (*31*) (DIPSI-2, τ_m 55 and 70 ms) spectra. Aromatic side chain resonances were assigned from 2D TOCSY (*32*) (τ_m 55 ms) and 2D NOESY spectra (*33*) (τ_m 100 ms) in D_2O as well as from a 3D ^{13}C-edited NOESY (τ_m 100 ms) spectrum. Estimation of $^3J_{HNH\alpha}$ values was obtained from an HNHA experiment (*34*). Distance information was collected from 2D NOESY (τ_m 100 ms), 3D ^{15}N-edited NOESY (*35*) (τ_m 100 ms), 3D ^{13}C-edited NOESY (*36*) (τ_m 100 ms), and 3D ^{13}C F_1-edited, F_3-filtered HMQC-NOESY (*37*) (τ_m 100 ms) spectra. H−D exchange data were obtained from a ^{15}N HSQC spectrum recorded after incubation of the sample in D_2O at 308 K for 1 h. Data were processed on a SGI Octane workstation using nmrPipe/nmrDraw (*38*) and analyzed using Sparky (T. D. Goddard and D. G. Kneller, UCSF).

Structure Calculations. Structures were calculated with the CNS 1.0 program (*39*) starting from an extended polypeptide chain using standard simulated annealing protocols with torsion angle dynamics. Prochiral groups were given floating stereospecific assignments and nonbonded contacts were represented by a quartic van der Waals repulsion term. Distance restraints were classified based on peak intensities as strong (1.8−2.7 Å), medium strong (1.8−3.1 Å), medium (1.8−3.5 Å), medium-weak (2.3−4.2 Å), weak (2.8−5.0 Å), and very weak (2.8−6.0 Å). Very weak NOE restraints were only used in cases in which the reciprocal NOE could be observed. Two restraints, 2.3−3.2 Å for r_{N-O} and 1.5−3.0 Å for r_{HN-O}, were used for each hydrogen bond. These were only included in the final stages of refinement and were based on a combination of NOE patterns and H−D exchange data. The crystal structure of the *E. coli* homologue, YjgF (*12*), was used to differentiate intersubunit NOEs from intrasubunit NOEs in the first instance, and these were subsequently confirmed using the 3D ^{13}C F_1-edited, F_3-filtered HMQC-NOESY data. Only intersubunit contacts that could be detected by NMR were used in the structure calculations. The final values used for the force constants were 1000 kcal mol^{-1} $Å^{-2}$ for bond lengths, 500 kcal mol^{-1} rad^{-2} for angles and improper torsions, 40 kcal mol^{-1} $Å^{-2}$ for experimental distance restraints, 200 kcal mol^{-1} rad^{-2} for dihedral restraints, and 4.0 kcal mol^{-1} $Å^{-4}$ for the van der Waals repulsion term. Noncrystallographic symmetry restraints were used with a force constant of 50 kcal mol^{-1} $Å^{-2}$. Structures were analyzed with PROCHECK−NMR (*40*) and QUANTA (Molecular Simulations, Inc.).

Ligand Screening. Compounds tested for binding to HI0719 are summarized in Table 1 and are based on at least one of the following published observations: an affect on isoleucine biosynthesis or threonine degradation (*5*−*7*, *11*), putative translation inhibition or ribonuclease activity (*1*−*3*), a potential role in purine regulation (*10*), and 2-amino-muconate deaminase activity (*17*−*20*). In addition, computational docking was used in an effort to gain further insights into the types of potential ligands (see below). All the test compounds were commercially available (Sigma-Aldrich, Fluka). Ligand screening was carried out by mixing test compounds with ^{15}N-labeled HI0719, recording ^{15}N HSQC spectra at 308 K, and comparing these spectra with a control spectrum of just the protein acquired using the same buffer conditions. Typical ligand-to-protein ratios were 3:1 with a 0.3 mM protein concentration. Some compounds, such as amino acids and nucleotides, were tested in groups of up to 20 at a time. The remaining small molecules were tested by adding them serially to a protein solution until an effect was observed with no more than seven compounds added per protein solution. Where no effect was detected, an established binder such as maleate or 2-ketobutyrate was added as a control to verify the binding competency of the protein. In all cases, care was taken to ensure that the pH was maintained after addition of the small molecules.

K_d Determination. The extent of binding of 2-ketobutyrate to HI0719 was determined by monitoring the change in chemical shifts of HSQC cross-peaks as a function of the 2-ketobutyrate concentration. To do this, a 0.6 mM solution of ^{15}N-labeled HI0719 in 20 mM Tris, 100 mM NaCl, 5 mM $MgCl_2$, and 3 mM DTT at pH 6.9 was titrated with a total of twenty 1-μL additions of 100 mM 2-ketobutyrate in 50 mM Bis-Tris pH 7.0 and ^{15}N HSQC spectra were recorded with each successive addition. The absolute value of the

Table 1: Test Compounds Screened for Binding to HI0719

basis for screening	test compounds[a]
Ile biosynthetic path	L-homoserine, 2-ketobutyrate, crotonate, tiglate, vinyl glycine, 2-aminobutyrate, 2-amino-1-propene-1,1,3-tricarbonitrile, methyl 3-aminocrotonate, methyl-2-hydroxy-2-methyl-3-oxobutyrate, 2-ethyl-2-hydroxybutyrate, 2-ethylbutyrate, ethylmalonate, 2-hydroxybutyrate, 2-hydroxy-3-methyl pentanoate, calcium pantothenate, 3-methyl-2-oxovalerate, 3-methyl-2-oxobutyrate, 2-oxopentanoate, propanoate, 3,3-dimethyl acrylate, thiamine pyrophosphate, *O*-phospho-DL-threonine, phospho(enol)pyruvate, *β*-hydroxypyruvate, methacrylate, pyridoxal phosphate
translation inhibition/ribonuclease activity/ purine regulation[b]	3′-AMP, 3′-CMP, 3′2′-GMP, 2′3′-UMP, 3′5′-cyclic AMP, 5′-ATP, 5′-ADP, 5′-AMP, 5′-CTP, 5′-CDP, 5′-CMP, 5′-GTP, 5′-GDP, 5′-GMP, 5′-UTP, 5′-UDP, 5′-UMP, 5′-TMP, 2′-deoxy 5′-GMP, 2′-deoxy 5′-AMP, 2′-deoxy 5′-CMP, adenosine, cytidine, uridine, guanosine, 2′-deoxyguanosine, 2′-deoxycytidine, 2′-deoxyadenosine, thymidine, cytosine, adenine, thymine, guanine, uracil, ribose, ribose 5-phosphate, all 20 naturally occurring amino acids, NADPH, coenzyme A, ascorbate
2-aminomuconate deaminase activity	2-aminothiazole, 2-oxoadipate, 2-aminoadipate, 2-amino-4- pentenoate, *cis*,*cis*-2,5-dimethyl muconate, maleate, 2-oxopentanedioate, maleic anhydride, glutaconate, fumarate
computational docking[c]	porphobilinogen (−36.8), α-D-xylose-1-phosphate (−35.0), *O*-phospho-L-serine (−33.5), 4- oxo-hepta-2,5-dienedioate (closest analogue −31.7), L-lysine (−30.3), 5-aminolevulinate (−29.8), 3-oxalomalate (−29.0), *cis*-aconitate (−27.0), *O*-phospho-L-tyrosine (−26.7), nalidixate (−25.3), D-glucosamine (−25.3), D-galactosamine (−24.3)

[a] The test compounds were dissolved in 50 mM bis-Tris at pH 7.0 and added to protein in 20 mM Tris, 100 mM NaCl, 0.3 mM $MgCl_2$, and 3 mM DTT at pH 6.9 unless otherwise noted. [b] The buffer used for the protein and test compounds in this category was 20 mM Tris, 100 mM NaCl, 0.3 mM $MgCl_2$, and 0.3 mM $CaCl_2$ at pH 6.7. [c] Numbers in brackets are DOCK binding energies.

difference in chemical shift of an atom with no 2-ketobutyrate present and that with 2-ketobutyrate added ($\Delta\delta_{obs}$) was plotted against the total amount of 2-ketobutyrate added (L_{tot}) and fitted with the equation:

$$\Delta\delta_{obs} = \Delta\delta_{max}\{(K_d + L_{tot} + E_{tot}) - [(K_d + L_{tot} + E_{tot})^2 - 4L_{tot}E_{tot}]^{1/2}\}/(2E_{tot}) \quad (1)$$

where $\Delta\delta_{max}$ is the maximum chemical shift difference seen for atoms of the protein saturated with 2-ketobutyrate, K_d is the dissociation constant, and E_{tot} is the total amount of HI0719 present in solution (*41*). The concentration of protein was verified by UV/Vis spectroscopy.

Computational Docking. Candidate ligands were drawn from the LIGAND database (*42*, *43*) of metabolites and their 3D starting structures and atomic charges were assigned with the program Concord (*44*), which uses Gasteiger-Marsili charges (*45*). The compounds were fitted to the hypothetical binding site with the program DOCK (*46*, *47*) and relative binding strengths were estimated by scoring with the force field energy, using AMBER (*48*, *49*) parameters for the receptor and modeling solvation with the 4r dielectric approximation. The compounds were classified according to their total charge and each class was ranked by force field score. Several representative high-scoring compounds from each charge-class were selected for experimental study.

RESULTS AND DISCUSSION

Oligomeric State in Solution. Following thrombin cleavage of the N-terminal $(His)_6$ tag from HI0719 on a native gel provides information about the oligomeric state of the protein. At an intermediate stage in the cleavage, four components will be present for a homotrimer—one where all three subunits have a tag, one where two of the subunits have a tag, one where one of the subunits has a tag, and one where complete cleavage has occurred and none of the subunits has a tag. The differences in mobilities for each of these components are sufficient that intermediate bands are readily resolved on the native gel and aliquots collected over time after addition of thrombin to HI0719 clearly showed four bands consistent with HI0719 being a trimer in solution. The trimeric quaternary structure of HI0719 was further confirmed using a combination of size exclusion chromatography and in-line laser light scattering (*50*).

Chemical Shift Assignments. No deuteration (*51*) or TROSY (*52*) experiments were required in our NMR analysis of HI0719. There is at least one other example in the literature, that of 4-oxalocrotonate tautomerase (4-OT), where detailed NMR analysis was done on a relatively large protein (ca. 41 kDa) without the use of deuteration or TROSY (*53*). Both 4-OT and HI0719 can be studied readily by NMR due to (i) the compact globular structures; (ii) the high concentrations attainable (≥3 mM); (iii) the high protein stabilities allowing temperatures of 35 °C (HI0719) or 42 °C (4-OT) to be used for data collection; and (iv) the simplified spectra from 3-fold (HI0719) or 6-fold (4-OT) symmetry. Assignments were obtained for nearly all (>98%) of the H_N, N, C_α, H_α, C_β, and H_β resonances in HI0719. The backbone H_N and ^{15}N shifts of only two residues, Asn26 and Cys109, could not be assigned. Side chain assignments beyond the C_β/H_β atoms were made for the majority of relevant residues although spectral overlap prevented C_γ/H_γ assignments in some cases. In particular, charged Arg, Lys, or Glu residues at the protein surface typically had partial assignments, and most of these contribute only a minimal number of side chain NOEs to the global fold. An exception to this was Lys117 for which complete assignment was made and the aliphatic chain of this residue is involved in extensive NOE contacts with the hydrophobic core. A complete list of chemical shift assignments has been deposited in the BioMagResBank (http://www.bmrb.wisc.edu/, accession number 5606).

Table 2: Summary of Statistics for the Ensemble of 20 Structures[a]

A. Experimental restraints	
distance restraints	
all NOE	1361
intraresidue	64
sequential ($\|i-j\|=1$)	388
medium-range ($1<\|i-j\|\leq 5$)	397
long-range ($\|i-j\|>5$)	417
intersubunit	95
hydrogen bond	99
dihedral angle restraints (ϕ)	58
B. RMSDs to mean structure (Å) for residues 1−130	
backbone atoms (N, C_α, CO)	0.85 ± 0.22
all non-hydrogen atoms	1.46 ± 0.24
C. Measures of structure quality (PROCHECK)	
most favored (%)	73.2 ± 2.1
additionally allowed (%)	21.9 ± 2.0
generously allowed (%)	3.5 ± 1.4
disallowed (%)	1.4 ± 0.7
number of bad contacts per 100 residues	5.2 ± 2.2
overall dihedral G factor	-0.34 ± 0.03

[a] Statistics quoted are the mean ± one standard deviation.

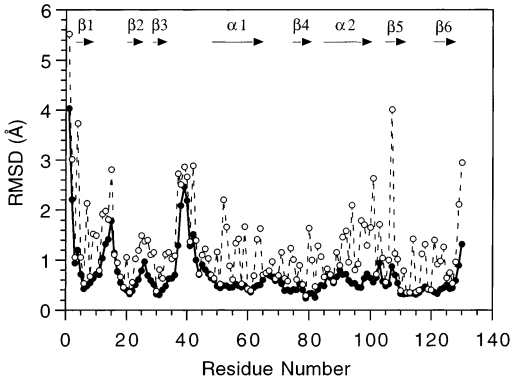

FIGURE 3: RMSD values per residue for the backbone (N, C_α, CO; filled circles, continuous line) and all non-hydrogen atoms (open circles, broken line).

Solution Structure of HI0719. The chemical shift index indicated the presence of six β-strands and two α-helices and these were subsequently confirmed during NOE analysis. An average of approximately 11 restraints per residue was used to calculate the final structure and the structure statistics are summarized in Table 2. The backbone and non-hydrogen atom RMSDs per residue for the final ensemble of 20 structures are shown in Figure 3. The overall structure (Figure 4) is well defined with an average backbone RMSD of 0.85 Å and the least determined regions correspond to the β1−β2 (residues 9−19) and β3−α1 (residues 32−46) loops. The intersubunit contacts found in the NMR structure were consistent with those in the crystal structures of the YjgF and YabJ homologues and, on the whole, the solution structure of HI0719 is similar to these crystal structures as evidenced by a C_α atom RMSD of 1.3 Å with the YjgF protein.

The hydrogen−deuterium exchange data on HI0719 further support the trimeric structure in solution. The backbone amide protons of Arg107, Glu111, Ala113, and Arg114 all have slowed exchange due to intersubunit hydrogen bonds (Figure 4, center panel). The backbone NH of Arg107 is within hydrogen bonding distance of the Ser31 Oγ atom in the adjacent subunit for both the solution and crystal structures. The other three residues are located in the β5−β6 loop and form the following intersubunit hydrogen bonds: Glu111 NH (subunit A)−Arg114 CO (subunit C), Ala113 NH (subunit A)−Glu111 CO (subunit B), and Arg114 NH (subunit A)−Glu111 CO (subunit B). This hydrogen bonding scheme is consistent with that found in the homologous crystal structures.

One of the most striking features of both the solution and X-ray structures is the presence of a cavity at the subunit interface containing six of the seven invariant residues in the high identity group (Figure 5). This cavity could potentially be a binding site for small molecules or short tracts of larger molecules and is suggestive of an enzymatic function. However, screening the PROCAT database (*54*) does not reveal any known enzyme structures with this type of residue arrangement in their active sites. Described below are our efforts to identify small molecules that bind in this cavity.

Test Compounds Based on the Isoleucine Biosynthetic Pathway. Since several homologues have been suggested to play a role in the regulation of isoleucine biosynthesis, we investigated whether HI0719 bound to any of the intermediates in this pathway. In cases in which specific intermediates were not readily available, structural analogues were used for ligand screening. Approximately 30 compounds in this category were tested for binding to HI0719, and the results

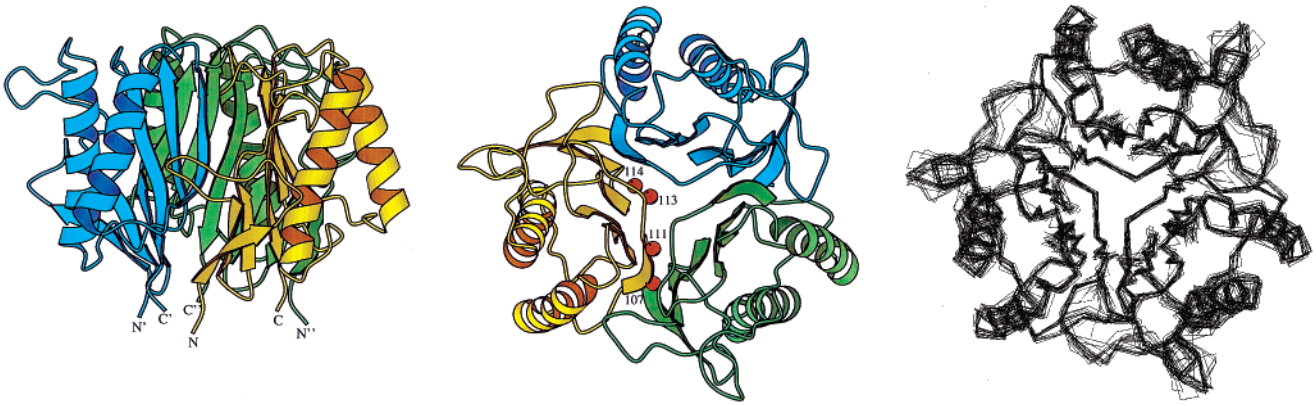

FIGURE 4: (Left panel) Molscript (*63*) ribbon diagram for the average structure showing the three subunits with a view of the intersubunit cleft. This view is at 90° to the 3-fold axis of symmetry. (Center panel) Ribbon diagram showing the view down the 3-fold axis of symmetry for the average structure. Subunits A, B, and C are colored yellow, blue, and green, respectively. The red spheres represent the positions of amide protons that are in slow exchange due to intersubunit hydrogen bonds as described in the text. Only those in subunit A are shown for clarity. (Right panel) The ensemble of 20 low energy final structures shown with the same view as in the center panel.

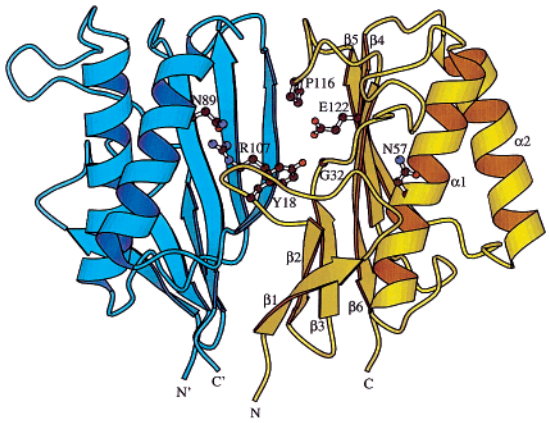

FIGURE 5: Ribbon diagram showing the view of the intersubunit cavity with the invariant residues mapped onto the structure. The view is the same as in Figure 4 (left panel) with the subunit at the rear omitted for clarity.

are summarized in Figure 6. Four compounds, 2-ketobutyrate (**1**), 2-ketoisovalerate (**2**), tiglate (**3**), and methacrylate (**4**) bound to HI0719 causing extensive perturbations in the ^{15}N-HSQC spectrum of the protein for residues Thr8, Ala13, Ile15, Gly16, Gly32, Gln33, Asp84, Ala86, Ala87, Val88, Asn89, Ala90, Glu93, Ser108, Lys117, and Gly120. The same cross-peaks were shifted for all four compounds although the change in shifts was largest for 2-ketobutyrate (Figure 7). Free and bound states were in fast exchange as evidenced by a single set of peaks due to HI0719 in the ^{15}N-HSQC spectra (Figure 8). Resonances affected by the addition of 2-ketobutyrate were mapped onto the three-dimensional structure showing that almost all of the perturbations are due to residues that are in or near the putative active site at the subunit interface (Figure 9). Using the three ^{15}N-HSQC cross-peaks with the largest shifts, Ile15, Gly16, and Val88, the dissociation constant for 2-ketobutyrate was estimated from eq 1 to be approximately 2 mM (Figure 10).

These results appear to point to the step in the isoleucine path where enamine (**8**) is converted to 2-ketobutyrate (**1**) (Figure 6). Only structural analogues of the enamine could be tested as it is quite unstable and not readily available. Tiglate (**3**) and methacrylate (**4**) both bind to HI0719 but if the 2-methyl group is removed, as in compounds **9** or **10**, no binding is observed. For 2-ketobutyrate analogues, the constraints for binding also appear to be narrow. Addition of a methyl group at the 3-position (**2**) results in binding, but addition of a methyl or carboxyl at the 4-position (**5** and **6**, respectively) leads to only very small changes in the HSQC spectrum as does substitution of the 2-keto group for a 2-hydroxy group (**7**). None of the other compounds tested in this category showed any affect on the chemical shifts of HI0719.

Test Compounds Based on Translation Inhibition and a Putative Role in Purine Regulation. It has been suggested that the rat homologue of HI0719 inhibits translation by acting as a ribonuclease which cleaves single-stranded RNA (*2*). The structure of HI0719 is not consistent with that of any known ribonuclease (see above) and, in our hands,

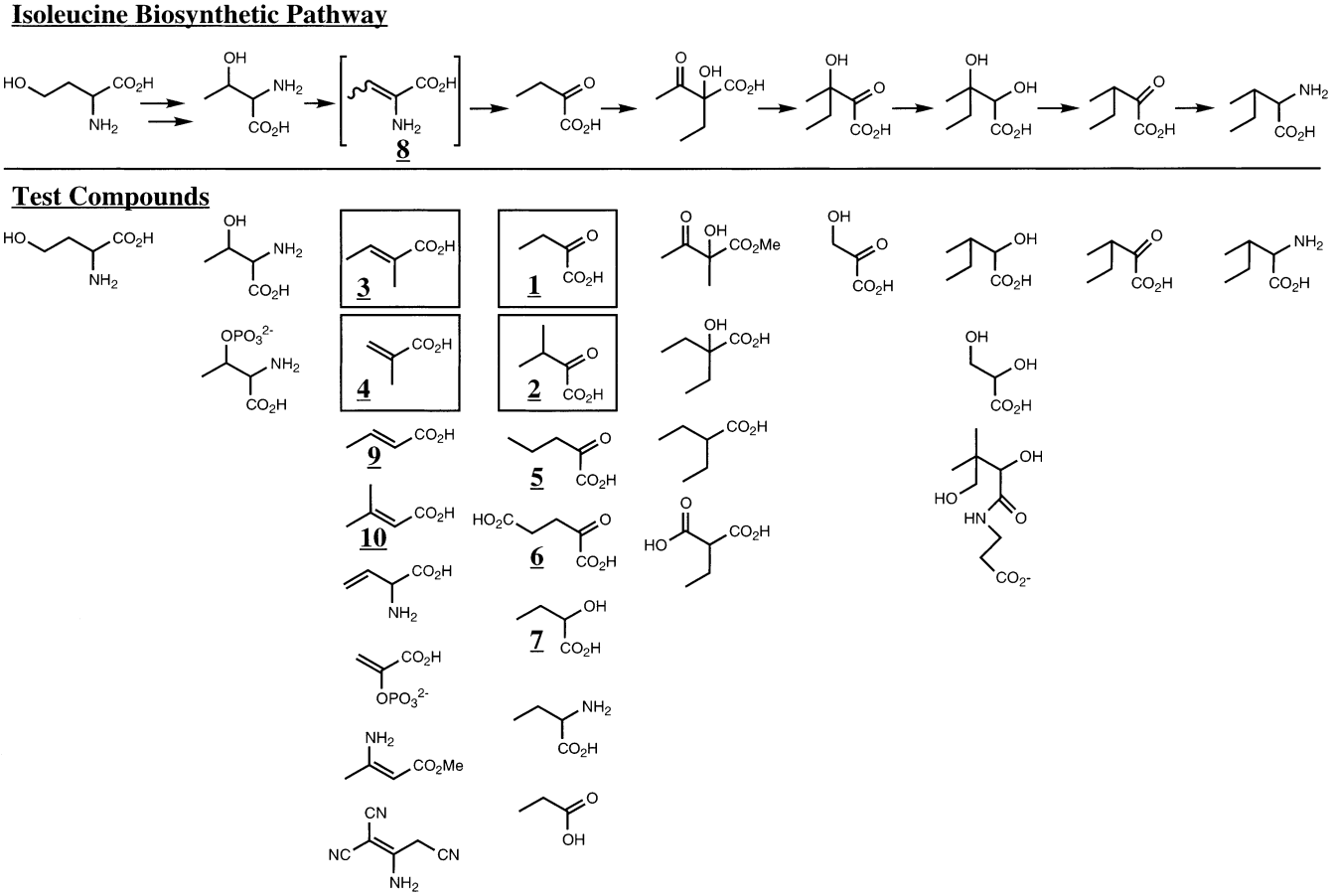

FIGURE 6: Summary of the isoleucine pathway and compounds tested for binding to HI0719. Compounds that caused significant changes in the ^{15}N HSQC spectrum of HI0719 are highlighted in boxes.

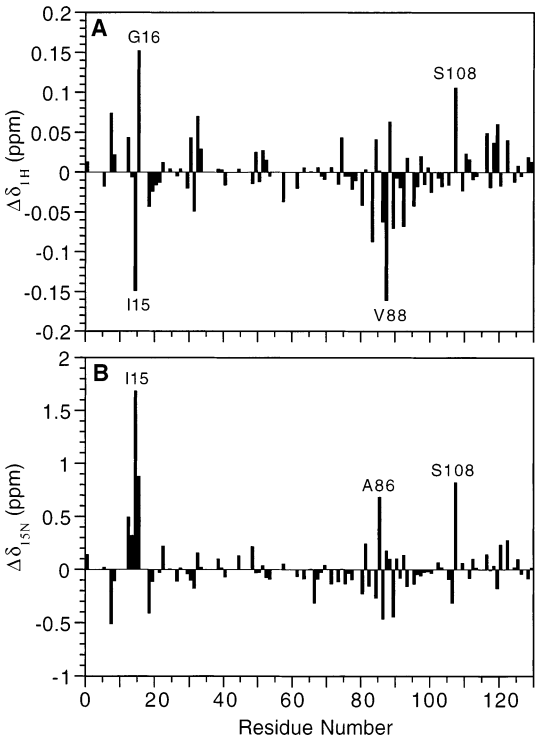

FIGURE 7: Chemical shift difference plots of (A) $\Delta\delta_{1H}$ ($= \delta_{control} - \delta_{ligand}$) and (B) $\Delta\delta_{15N}$ versus residue number when the 2-ketobutyrate/protein ratio is 3:1.

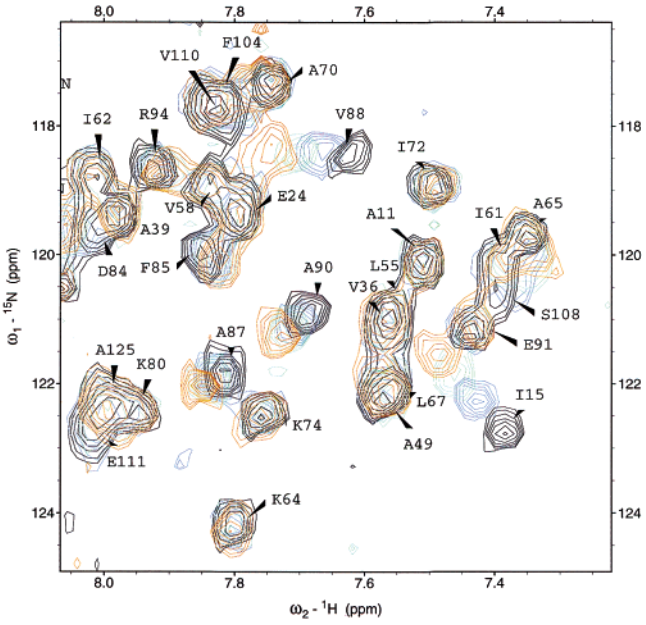

FIGURE 8: Section of the overlayed ^{15}N HSQC spectra of HI0719 (0.3 mM) acquired with different amounts of 2-ketobutyrate (2kb) as follows: control (black); 0.2 mM 2kb (blue); 0.4 mM 2kb (green); 0.6 mM 2kb (red).

HI0719 did not exhibit any ribonuclease activity (data not shown). Proposals have also been made that the *B. subtilis* homologue, YabJ, plays a role in purine regulation (*10*). On the basis of both the translation inhibition and purine regulation observations, we tested HI0719 for binding to a wide range of small molecules that are summarized in Table 1. Experiments were done in the presence and absence of divalent cations (Mg^{2+} and/or Ca^{2+}), but no binding was detected.

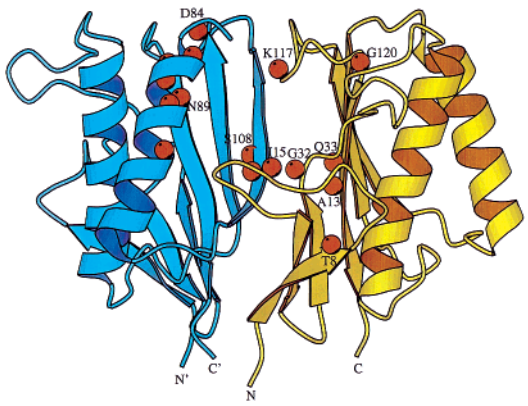

FIGURE 9: Ribbon diagram showing the location of amide groups (red spheres) in HI0719 that have perturbed chemical shifts when 2-ketobutyrate is added. Only residues that display significant changes in chemical shifts ($\geq$0.05 ppm for ^1H_N and/or $\geq$0.5 ppm for ^{15}N) are shown and data are taken from the plots in Figure 7. The view is the same as in Figure 5 with the rear subunit omitted for clarity.

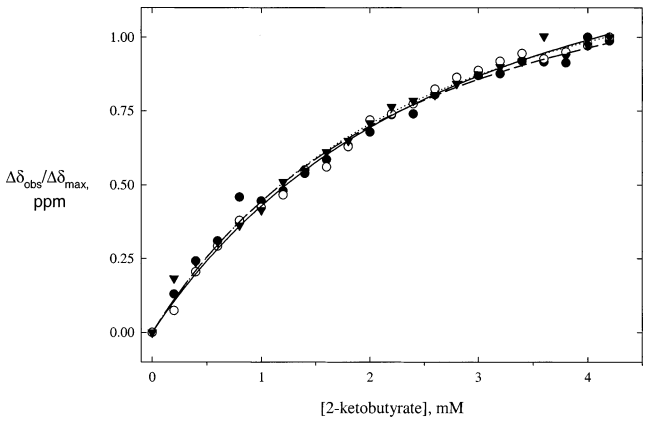

FIGURE 10: Binding curves for 2-ketobutyrate using the ^1H_N shifts of Ile15 (filled circles), Gly16 (triangles), and Val88 (open circles).

Test Compounds Based on 2-Aminomuconate Deaminase Activity. The low identity homologue of HI0719, 2-aminomuconate deaminase, has been shown to convert 2-aminomuconate (**11**) to 4-oxalocrotonate (**12**) (Figure 11A) as the ammonia releasing step in the degradation of nitrobenzene (*17*−*20*). Four of the six invariant residues in the putative active site of HI0719 and its high identity homologues are maintained in the 2-aminomuconate deaminases based on sequence alignment (see http://s2f.umbi.umd.edu/). Because of these similarities in the putative active sites, it may be possible that the high identity HI0719 family of proteins interact with small molecules that are structurally related to the substrate and product of 2-aminomuconate deaminase and carry out similar chemistry. On the basis of these observations, a number of readily available structural analogues of **11** and **12** were tested (Table 1). Two of these, maleate (**13**) and maleic anhydride (**14**), did bind to HI0719 with similar affinities to compounds **1**−**4** and also with almost identical changes in the HSQC spectrum. In contrast, the trans isomer, fumarate, showed no sign of binding to HI0719. After the ligand screening experiments, HI0719 was directly tested for 2-aminomuconate deaminase activity but was found to be inactive (Dr. Hak-Sung Kim, personal communication).

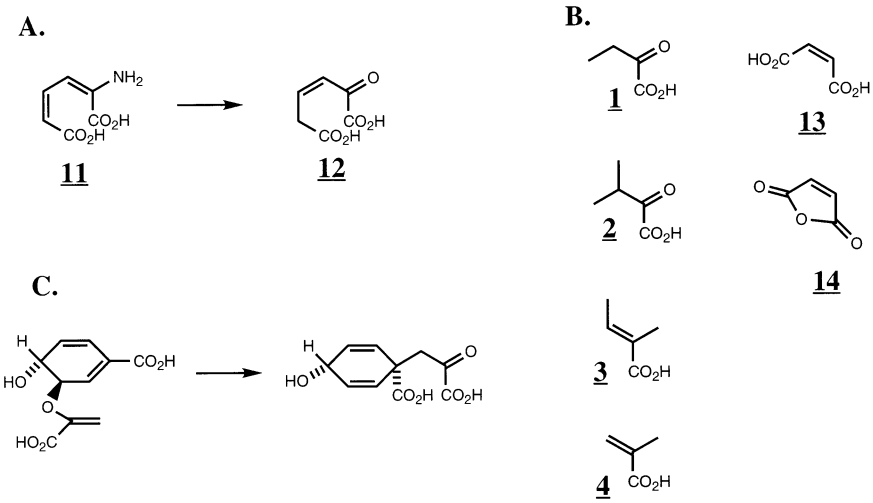

FIGURE 11: (A) The step in nitrobenzene degradation catalyzed by 2-aminomuconate deaminase. (B) Structures for the compounds shown to bind HI0719 at the putative active site. (C) The conversion of chorismate to prephenate catalyzed by chorismate mutase.

Test Compounds Based on Computational Docking. Candidate ligands from computational docking were sorted into bins based on charge (−3, −2, −1, 0, +1, +2) and compounds containing phosphorus or sulfur were put in a separate category. The range of DOCK binding energies (quoted in "DOCK units") for the top 10 candidates in each category was as follows: −3 (−29.6 to −25.3), −2 (−36.7 to −24.8), −1 (−36.8 to −25.3), 0 (−34.4 to −29.2), +1 (−30.3 to −24.0), and phosphorus/sulfur (−37.4 to −33.3). The +2 bin contained only four compounds with negative DOCK binding energies (−23.0 to −20.1) and this bin was not considered further due to the less favorable binding energies. The top 10 candidates from the other bins were assessed for their commercial availability and the readily available compounds among these (about 2−3 compounds per bin on average) were tested accordingly. The compounds tested and their DOCK binding energies to the putative active site of HI0719 are summarized in Table 1. None of these compounds bound under the conditions used, but it is interesting to note the computational binding energies of the other naturally occurring compounds (**1**, **2**, **13**) that did bind. 2-Ketobutyrate (**1**) and 2-ketoisovalerate (**2**) have DOCK binding energies of −6.8 and −7.5, respectively, while maleate (**13**) ranks 13th in the −2 bin with a value of −23.8. These three compounds all bound HI0719 with comparable affinities. Therefore, no clear correlation exists between the computational predictions and the experimental results of ligand binding within this limited data set.

CONCLUSIONS

The solution structure of HI0719 is consistent with the previously reported crystal structures of other high identity homologues and shows a cavity lined with invariant residues that is likely to be a binding site for small molecules. The ligand screening study was able to identify six small molecules that bind to HI0719 at the putative active site (Figure 11B). Five of these compounds are either α-keto acids or α,*β*-unsaturated acids, while the sixth compound is structurally similar. Four of the binders (**1**−**4**) were based on intermediates in the isoleucine pathway and it is this path that appears to have the most connections to cellular functions reported in the literature. If HI0719 or any of its high identity group homologues acts on any small molecules in the isoleucine biosynthetic path as has been proposed, then our results suggest that the interaction most likely occurs at the step where the unstable enamine (**8**) is deaminated to form 2-ketobutyrate (**1**) (Figure 6). Although threonine deaminase *dehydrates* threonine to enamine (**8**), no enzyme has been found for the deamination of **8** to **1**, which raises the possibility that the function of HI0719 and its homologues is to catalyze this step. However, because tautomerization of (**8**) to its imine and subsequent hydrolysis to (**1**) occur spontaneously in aqueous solution (*55*), no enzyme should be needed to accelerate this step. Another possibility is that HI0719 acts on **8** and/or **1** to regulate their levels either by binding them to buffer their intracellular concentration or by an as yet undefined mechanism. Further experiments will be necessary to test these possibilities. 2-Ketobutyrate is a regulatory metabolite that is known to affect other pathways (*56*−*58*), and this may help to explain the complex phenotypes that have been observed when the yjgF gene is mutated or deleted (*11*).

The resemblance of the step in isoleucine biosynthesis identified by ligand screening to the reaction carried out by 2-aminomuconate deaminase (Figure 11A) is readily apparent. Both reactions involve the conversion of an α,*β*-unsaturated amino acid into an α-keto acid suggesting that the molecular functions of HI0719 and 2-aminomuconate deaminase are related. It is interesting to note that the substrate and product of the more distantly related chorismate mutase appear to have some weak structural similarity to the substrate and product from 2-aminomuconate deaminase (Figure 11C) as well as to compounds **1**−**4** from screening of isoleucine pathway intermediates. This, in combination with the similar folds, would suggest that all these proteins evolved from the same family and diverged to give their related but distinct ligand specificities.

The targeted ligand screening method used here does not give a definitive molecular function for the HI0719 family but is nonetheless a powerful approach because it narrows down the potential ligands for this protein and is amenable to high throughput methods for ligand screening by NMR. The advent of cryogenic probes (*59*) coupled with flow technology (*60*) will make this type of functional ligand

screening more efficient as will be needed to deal with the large number of proteins with no known function that have been found through genome sequencing efforts.

ACKNOWLEDGMENT

We thank Dr. Jim Parsons for his advice on cloning, expression, and purification. Eugene Melamud and Dr. John Moult are gratefully acknowledged for maintaining the web site for this project (http://s2f.umbi.umd.edu/). We also thank Dr. Hak-Sung Kim of the Korean Advanced Institute of Science and Technology for carrying out the assay for 2-aminomuconate deaminase activity. The NMR facility at CARB is supported in part by grants from the W. M. Keck Foundation and the NIH Shared Instrumentation Program (1S10RR15744).

REFERENCES

1. Schmiedeknecht, G., Kerkhoff, C., Orso, E., Stohr, J., Aslanidis, C., Nagy, G. M., Knuechel, R., and Schmitz, G. (1996) Isolation and characterization of a 14.5-kDa trichloroacetic-acid-soluble translational inhibitor protein from human monocytes that is upregulated upon cellular differentiation. *Eur. J. Biochem. 242*, 339−351.
2. Morishita, R., Kawagoshi, A., Sawasaki, T., Madin, K., Ogasawara, T., Oka, T., and Endo, Y. (1999) Ribonuclease activity of rat liver perchloric acid-soluble protein, a potent inhibitor of protein synthesis. *J. Biol. Chem. 274*, 20688−20692.
3. Oka, T., Nishimoto, Y., Sasagawa, T., Kanouchi, H., Kawasaki, Y., and Natori, Y. (1999) Production of functional rat liver PSP protein in *Escherichia coli*. *Cell. Mol. Life Sci. 55*, 131−134.
4. Oxelmark, E., Marchini, A., Malanchi, I., Magherini, F., Jaquet, L., Hajibagheri, M. A., Blight, K. J., Jauniaux, J. C., and Tommasino, M. (2000) Mmf1p, a novel yeast mitochondrial protein conserved throughout evolution and involved in maintenance of the mitochondrial genome. *Mol. Cell. Biol. 20*, 7784−7797.
5. Kim, J. M., Yoshikawa, H., and Shirahige, K. (2001) A member of the YER057c/yjgf/Uk114 family links isoleucine biosynthesis and intact mitochondria maintenance in *Saccharomyces cerevisiae*. *Genes Cells 6*, 507−517.
6. Goupil-Feuillerat, N., Cocaign-Bousquet, M., Godon, J. J., Ehrlich, S. D., and Renault, P. (1997) Dual role of alpha-acetolactate decarboxylase in *Lactococcus lactis* subsp. lactis. *J. Bacteriol. 179*, 6285−6293.
7. Hesslinger, C., Fairhurst, S. A., and Sawers, G. (1998) Novel keto acid formate-lyase and propionate kinase enzymes are components of an anaerobic pathway in *Escherichia coli* that degrades L-threonine to propionate. *Mol. Microbiol. 27*, 477−492.
8. Melloni, E., Michetti, M., Salamino, F., and Pontremoli, S. (1998) Molecular and Functional Properties of a Calpain Activator Protein Specific for μ-Isoforms. *J. Biol. Chem. 273*, 12827−12831.
9. Ceciliani, F., Faotto, L., Negri, A., Colombo, I., Berra, B., Bartorelli, A., and Ronchi, S. (1996) The primary structure of UK114 tumor antigen. *FEBS Lett. 393*, 147−150.
10. Rappu, P., Shin, B. S., Zalkin, H., and Mantsala, P. (1999) A role for a highly conserved protein of unknown function in regulation of *Bacillus subtilis* purA by the purine repressor. *J. Bacteriol. 181*, 3810−3815.
11. Enos-Berlage, J. L., Langendorf, M. J., and Downs, D. M. (1998) Complex metabolic phenotypes caused by a mutation in yjgF, encoding a member of the highly conserved YER057c/YjgF family of proteins. *J. Bacteriol. 180*, 6519−6528.
12. Volz, K. (1999) A test case for structure-based functional assignment: The 1.2 Å crystal structure of the yjgF gene product from *Escherichia coli*. *Protein Sci. 8*, 2428−2437.
13. Sinha, S., Rappu, P., Lange, S. C., Mantsala, P., Zalkin, H., and Smith, J. L. (1999) Crystal structure of *Bacillus subtilis* YabJ, a purine regulatory protein and member of the highly conserved YjgF family. *Proc. Natl. Acad. Sci. U.S.A. 96*, 13074−13079.
14. Deaconescu, A. M., Roll-Mecak, A., Bonanno, J. B., Gerchman, S. E., Kycia, H., Studier, F. W., and Burley, S. K. (2002) X-ray structure of *Saccharomyces cerevisiae* homologous mitochondrial matrix factor 1 (Hmf1). *Proteins 48*, 431−436.
15. Oka, T., Tsuji, H., Noda, C., Sakai, K., Hong, Y. M., Suzuki, I., Munoz, S., and Natori, Y. (1995) Isolation and characterization of a novel perchloric acid-soluble protein inhibiting cell-free protein synthesis. *J. Biol. Chem. 270*, 30060−30067.
16. Chook, Y. M., Gray, J. V., Ke, H., and Lipscomb, W. N. (1994) The monofunctional chorismate mutase from *Bacillus subtilis*. Structure determination of chorismate mutase and its complexes with a transition state analogue and prephenate, and implications for the mechanism of the enzymatic reaction. *J. Mol. Biol. 240*, 476−500.
17. He, Z., and Spain, J. C. (1997) Studies of the catabolic pathway of degradation of nitrobenzene by Pseudomonas pseudoalcaligenes JS45: removal of the amino group from 2-aminomuconic semialdehyde. *Appl. Environ. Microbiol. 63*, 4839−4843.
18. He, Z., and Spain, J. C. (1998) A novel 2-aminomuconate deaminase in the nitrobenzene degradation pathway of *Pseudomonas pseudoalcaligenes* JS45. *J. Bacteriol. 180*, 2502−2506.
19. Takenaka, S., Murakami, S., Shinke, R., and Aoki, K. (1998) Metabolism of 2-aminophenol by Pseudomonas sp. AP-3: modified meta-cleavage pathway. *Arch. Microbiol. 170*, 132−137.
20. Park, H. S., and Kim, H. S. (2000) Identification and characterization of the nitrobenzene catabolic plasmids pNB1 and pNB2 in *Pseudomonas putida* HS12. *J. Bacteriol. 182*, 573−580.
21. Shuker, S. B., Hajduk, P. J., Meadows, R. P., and Fesik, S. W. (1996) Discovering high-affinity ligands for proteins: SAR by NMR. *Science 274*, 1531−1534.
22. Parsons, L., Eisenstein, E., and Orban, J. (2001) Solution structure of HI0257, a bacterial ribosome binding protein. *Biochemistry 40*, 10979−10986.
23. Bax, A., and Pochapsky, S. S. (1992) Optimized recording of heteronuclear multidimensional NMR spectra using pulsed field gradients. *J. Magn. Reson. 99*, 638−643.
24. Mori, S., Abeygunawardana, C., Johnson, M. O., and van Zijl, P. C. (1995) Improved sensitivity of HSQC spectra of exchanging protons at short interscan delays using a new fast HSQC (FHSQC) detection scheme that avoids water saturation [published erratum appears in *J. Magn. Reson. B* 1996 Mar; *110* (3): 321]. *J. Magn. Reson. B 108*, 94−98.
25. Grzesiek, S., and Bax, A. (1992) Improved 3D triple-resonance NMR techniques applied to a 31 kDa protein. *J. Magn. Reson. 96*, 432−440.
26. Wittekind, M., and Mueller, L. (1993) HNCACB, a high sensitivity 3D NMR experiment to correlate amide-proton and nitrogen resonances with the alpha and beta carbon resonances in proteins. *J. Magn. Reson. Ser. B 101*, 201−205.
27. Grzesiek, S., and Bax, A. (1992) Correlating backbone amide and side chain resonances in larger proteins by multiple relayed triple resonance NMR. *J. Am. Chem. Soc. 114*, 6291−6293.
28. Vuister, G. W., and Bax, A. (1992) Resolution enhancement and spectral editing of uniformly ^{13}C-enriched proteins by homonuclear broadband ^{13}C decoupling. *J. Magn. Reson. 98*, 428−435.
29. Bax, A., Clore, G. M., Driscoll, P. C., Gronenborn, A. M., Ikura, M., and Kay, L. E. (1990) Practical aspects of proton-carbon−carbon-proton three-dimensional correlation spectroscopy of ^{13}C-labeled proteins. *J. Magn. Reson. 87*, 620−627.
30. Kay, L. E., Ikura, M., and Bax, A. (1990) Proton−proton correlation via carbon−carbon couplings: A three-dimensional NMR approach for the assignment of aliphatic resonances in proteins labeled with carbon-13. *J. Am. Chem. Soc. 112*, 888−889.
31. Marion, D., Driscoll, P. C., Kay, L. E., Wingfield, P. T., Bax, A., Gronenborn, A. M., and Clore, G. M. (1989) Overcoming the overlap problem in the assignment of ^{1}H NMR spectra of larger proteins using three-dimensional homonuclear Hartmann−Hahn and nuclear Overhauser ^{1}H-^{15}N heteronuclear multiple quantum coherence spectroscopy. *Biochemistry 29*, 6150−6156.
32. Braunschweiler, L., and Ernst, R. R. (1983) Coherence transfer by isotropic mixing: Application to proton correlation spectroscopy. *J. Magn. Reson. 53*, 521−528.
33. Kumar, A., Ernst, R. R., and Wuthrich, K. (1980) A two-dimensional nuclear Overhauser enhancement (2D NOE) experiment for the elucidation of complete proton−proton cross-relaxation networks in biological macromolecules. *Biochem. Biophys. Res. Commun. 95*, 1−6.
34. Vuister, G. W., and Bax, A. (1993) Quantitative J correlation: A new approach for measuring homonuclear three-bond J($H^{N}H^{\alpha}$) coupling constants in ^{15}N-enriched proteins. *J. Am. Chem. Soc. 115*, 7772−7777.

35. Fesik, S. W., and Zuiderweg, E. R. P. (1988) Heteronuclear three-dimensional NMR spectroscopy: a strategy for the simplification of homonuclear two-dimensional NMR spectra. *J. Magn. Reson. 78*, 588−593.
36. Ikura, M., Kay, L. E., Tschudin, R., and Bax, A. (1990) Three-dimensional NOESY−HMQC spectroscopy of a ^{13}C-labeled protein. *J. Magn. Reson. 86*, 204−209.
37. Lee, W., Revington, M. J., Arrowsmith, C., and Kay, L. E. (1994) A pulsed field gradient isotope-filtered 3D ^{13}C HMQC−NOESY experiment for extracting intermolecular NOE contacts in molecular complexes. *FEBS Lett. 350*, 87−90.
38. Delaglio, F., Grzesiek, S., Vuister, G. W., Zhu, G., Pfeifer, J., and Bax, A. (1995) NMRPipe: a multidimensional spectral processing system based on UNIX pipes. *J. Biomol. NMR 6*, 277−293.
39. Brunger, A. T., Adams, P. D., Clore, G. M., DeLano, W. L., Gros, P., Grosse, K. R., Jiang, J. S., Kuszewski, J., Nilges, M., Pannu, N. S., Read, R. J., Rice, L. M., Simonson, T., and Warren, G. L. (1998) Crystallography & NMR system: A new software suite for macromolecular structure determination. *Acta Crystallogr. D (Biol. Crystallogr.) 54*, 905−921.
40. Laskowski, R. A., Rullmann, J. A., MacArthur, M. W., Kaptein, R., and Thornton, J. M. (1996) AQUA and PROCHECK−NMR: Programs for checking the quality of protein structures solved by NMR. *J. Biomol. NMR 8*, 477−486.
41. Harris, T. K., Czerwinski, R. M., Johnson, W. H., Jr., Legler, P. M., Abeygunawardana, C., Massiah, M. A., Stivers, J. T., Whitman, C. P., and Mildvan, A. S. (1999) Kinetic, stereochemical, and structural effects of mutations of the active site arginine residues in 4-oxalocrotonate tautomerase. *Biochemistry 38*, 12343−12357.
42. Goto, S., Nishioka, T., and Kanehisa, M. (1998) LIGAND: chemical database for enzyme reactions. *Bioinformatics 14*, 591−599.
43. Kanehisa, M., Goto, S., Kawashima, S., and Nakaya, A. (2002) The KEGG databases at GenomeNet. *Nucleic Acids Res. 30*, 42−46.
44. Rusinko, A., Skell, J. M., Balducci, R., and Pearlman, R. S. CONCORD − Rapid generation of high quality approximate 3-dimensional molecular coordinates, Abstracts of papers of the American Chemical Society 192: 12-COMP SEP 7 1986.
45. Gasteiger, J., and Marsili, M. (1980) Iterative partial equalization of orbital electronegativity − A rapid access to atomic charges. *Tetrahedron 36*, 3219−3228.
46. Kuntz, I. D., Blaney, J. M., Oatley, S. J., Langridge, R., and Ferrin, T. E. (1982) A geometric approach to macromolecule-ligand interactions. *J. Mol. Biol. 161*, 269−288.
47. Ewing, T. J., Makino, S., Skillman, A. G., and Kuntz, I. D. (2001) DOCK 4.0: search strategies for automated molecular docking of flexible molecule databases. *J. Comput. Aided Mol. Des. 15*, 411−428.
48. Weiner, S. J., Kollman, P. A., Case, D. A., Singh, U. C., Ghio, C., Alagona, G., Profeta, S., and Weiner, P. (1984) A new force field for molecular mechanical simulation of nucleic acids and proteins. *J. Am. Chem. Soc. 106*, 765−784.
49. Cornell, W. D., Cieplak, P., Bayly, C. I., Gould, I. R., Merz, K. M., Ferguson, D. M., Spellmeyer, D. C., Fox, T., Caldwell, J. W., and Kollman, P. A. (1995) A second generation force field for the simulation of proteins, nucleic acids, and organic molecules. *J. Am. Chem. Soc. 117*, 5179−5197.
50. Folta-Stogniew, E., and Williams, K. R. (1999) Determination of molecular masses of proteins in solution: implementation of an HPLC size exclusion chromatography and laser light scattering service in a core laboratory. *J. Biomol. Technol. 10*, 51−63.
51. Yamazaki, T., Lee, W., Arrowsmith, C. H., Muhandiram, D. R., and Kay, L. E. (1994) A suite of triple resonance NMR experiments for the backbone assignment of ^{15}N, ^{13}C, ^{2}H labeled proteins with high sensitivity. *J. Am. Chem. Soc. 116*, 11655−11666.
52. Pervushin, K., Riek, R., Wider, G., and Wuthrich, K. (1997) Attenuated T2 relaxation by mutual cancellation of dipole−dipole coupling and chemical shift anisotropy indicates an avenue to NMR structures of very large biological macromolecules in solution. *Proc. Natl. Acad. Sci. U.S.A. 94*, 12366−71.
53. Stivers, J. T., Abeygunawardana, C., Whitman, C. P., and Mildvan, A. S. (1996) 4-Oxalocrotonate tautomerase, a 41-kDa homohexamer: backbone and side-chain resonance assignments, solution secondary structure, and location of active site residues by heteronuclear NMR spectroscopy. *Protein Sci. 5*, 729−741.
54. Wallace, A. C., Borkakoti, N., and Thornton, J. M. (1997) TESS: a geometric hashing algorithm for deriving 3D coordinate templates for searching structural databases. Application to enzyme active sites. *Protein Sci. 6*, 2308−2323.
55. Walsh, C. (1979) *Enzymatic Reaction Mechanisms*; W. H. Freeman, San Francisco.
56. Daniel, J., Dondon, L., and Danchin, A. (1983) 2-Ketobutyrate: a putative alarmone of *Escherichia coli*. *Mol. Gen. Genet. 190*, 452−458.
57. Danchin, A., Dondon, L., and Daniel, J. (1984) Metabolic alterations mediated by 2-ketobutyrate in *Escherichia coli* K12. *Mol. Gen. Genet. 193*, 473−478.
58. LaRossa, R. A., and Van Dyk, T. K. (1984) Metabolic mayhem caused by 2-ketoacid imbalances, *BioEssays 7*, 125−130.
59. Black, R. D., Early, T. A., Roemer, P. B., Mueller, O. M., Mogro-Campero, A., Turner, L. G., and Johnson, G. A. (1993) A high-temperature superconducting receiver for nuclear magnetic resonance spectroscopy. *Science 259*, 793.
60. Stockman, B. J., Farley, K. A., and Angwin, D. T. (2001) Screening of compound libraries for protein binding using flow-injection nuclear magnetic resonance spectroscopy. *Methods Enzymol. 338*, 230−246.
61. Altschul, S. F., Madden, T. L., Schaffer, A. A., Zhang, J., Zhang, Z., Miller, W., and Lipman, D. J. (1997) Gapped BLAST and PSI−BLAST: a new generation of protein database search programs. *Nucleic Acids Res. 25*, 3389−3402.
62. Thompson, J. D., Higgins, D. G., and Gibson, T. J. (1994) CLUSTAL W: improving the sensitivity of progressive multiple sequence alignment through sequence weighting, position-specific gap penalties and weight matrix choice. *Nucleic Acids Res. 22*, 4673−4680.
63. Kraulis, P. J. (1991) MOLSCRIPT: a program to produce both detailed and schematic plots of protein structures. *J. Appl. Crystallogr. 24*, 946−950.

BI020541W